Histol Histopathol (2022) 37: 1213-1226

http://www.hh.um.es

Histology and Histopathology
From Cell Biology to Tissue Engineering

ORIGINAL ARTICLE **Open Access**

Anesthetic propofol suppresses growth and metastasis of lung adenocarcinoma *in vitro* through downregulating circ-MEMO1-miR-485-3p-NEK4 ceRNA axis

Lei Chen, Guangyi Wu, Yongle Li and Qiaoying Cai

Department of Anesthesiology, Affiliated Hospital of Hebei University, Baoding City, Hebei Province, China

Summary. Background. Recently, circular RNAs (circRNAs) have been emerging as new regulators in the propofol-induced tumor-suppressive role. Here, we intended to investigate the involvement of circRNA-Mediator of cell motility 1 (circ-MEMO1; hsa_circ_0007385) in propofol role in cancer hallmarks of lung adenocarcinoma (LUAD).

Methods. Real-time quantitative PCR and western blotting examined transcriptional and translational levels of circ-MEMO1, microRNA (miR)-485-3p, and NIMA-related kinase-4 (NEK4), and markers of growth and metastasis including E-cadherin, CyclinD1, and Vimentin. Cancer hallmarks were measured by 3-(4, 5-dimethylthiazol-2-yl)-2,5-diphenyltetrazolium bromide assay, flow cytometry, 5-ethynyl-2-deoxyuridine assay, and transwell assay. The interaction among circ-MEMO1, miR-485-3p, NEK4 was determined by dual-luciferase reporter assay and Pearson's correlation analysis.

Results. Circ-MEMO1 and NEK4 were high-expressed, and miR-485-3p was low-expressed in LUAD patients and cells; moreover, circ-MEMO1 and NEK4 expression in LUAD cells could be suppressed, whereas miR-485-3p could be elevated with propofol anesthesia. Functionally, propofol restrained cell viability, cell cycle entrance, cell proliferation, migration, and invasion of LUAD cells, accompanied by promoted E-cadherin and depressed CyclinD1 and Vimentin. Coincidently, high circ-MEMO1 was associated with low overall survival of LUAD patients, and overexpressing circ-MEMO1 could overall attenuate propofol effects in LUAD cells. Of note, upregulating miR-485-3p and/or interfering NEK4 could partially countermand the adverse impacts of circ-MEMO1 on propofol's role in LUAD cells. Importantly, circ-MEMO1 acted as a sponge for miR-485-3p to modulate the expression of miR-485-3p-targeted oncogene NEK4.

Conclusion. Promoting the circ-MEMO1-miR-485-3p-NEK4 axis might halt the tumor-inhibiting role of propofol in LUAD cells *in vitro*, suggesting a potential epigenetic pathway of propofol.

Key words: Propofol, circ-MEMO1, miR-485-3p, NEK4, LUAD

Introduction

Propofol (2,6-diisopropylphenol) is one of the most widely used intravenous anesthetics in surgery for sedation and general anesthesia (Sahinovic et al., 2018). Notably, propofol has been noticed to serve additional non-anesthetic effects during surgery, such as the anticancer effect (Wang et al., 2018; Longhini et al., 2020). The increasing number of studies demonstrate that propofol per se could not only suppress tumor development but also enhance the anti-tumor effect of chemotherapeutic drugs or molecules (Xu et al., 2020). Propofol-based total intravenous anesthesia in oncologic surgery improves patients' survival outcomes through displaying anti-oxidation, anti-inflammation, anti-immunosuppression, etc. (Cassinello et al., 2015; Kim, 2017; Irwin et al., 2020). Mechanically, genetic signaling pathways and epigenetic pathways involving non-coding RNAs have been molecular mechanisms underlying propofol's malignance-modulating properties (Wang et al., 2018; Farooqi et al., 2020).

MicroRNAs (miRNAs) and long non-coding RNAs (lncRNAs) are two types of endogenous non-coding RNAs that could be regulated by propofol in cancer progression (Jiang et al., 2018b). Circular RNAs (circRNAs) are another special class of non-coding RNAs that are characterized by a covalently closed loop structure without a 5' cap and 3' poly-adenylated tails (Ng et al., 2018). Recently, several circRNAs have been unveiled to be abnormally expressed by propofol anesthesia (Sui et al., 2020; Wang et al., 2020; Zhao et

Corresponding Author: Yongle Li, MM, Department of Anesthesiology, Affiliated Hospital of Hebei University, No. 212 Yuhua East Road, Baoding 071000, Hebei Province, China. e-mail: li-yongle@163.com
DOI: 10.14670/HH-18-465

al., 2020), and these circRNAs dysregulations could suppress the anticancer role of propofol. Non-coding RNAs including circRNAs, lncRNAs, and miRNAs, are critical regulators, therapeutic targets and diagnostic biomarkers in human diseases (Beermann et al., 2016; Santos et al., 2020), including lung cancer which is one of the deadliest forms of cancer affecting society today.

Precisely, miRNAs and lncRNAs have been studied for decades, whilst renewed attention has been swerved towards circRNAs more recently (Ishola et al., 2020). Circular RNA mediator of cell motility 1 (circ-MEMO1; ID: hsa_circ_0007385) is an oncogene in non-small cell lung cancer (NSCLC) tumorigenesis (Jiang et al., 2018a), and shows clinical application value for disease monitoring and prognosis prediction in NSCLC patients (Lin et al., 2020). However, whether there was an association between propofol's anticancer role and circ-MEMO1 remains unfathomed.

Therefore, we aimed to investigate the expression and role of circ-MEMO1 in propofol anesthesia-induced inhibitory activities against lung adenocarcinoma (LUAD), a predominant subtype of NSCLC. Notably, lung cancer-related circRNA-miRNA-mRNA regulatory network is well-elaborated lately (Liang et al., 2020). Besides, a panel of miRNAs including miRNA (miR)-485-3p are molecular features to distinguish young LUAD patients (Giordano et al., 2018). NIMA-related kinase-4 (NEK4) gene maps to a commonly deleted locus in NSCLC (Doles and Hemann, 2010), and encodes a serine/threonine-protein kinase that is closely linked to NSCLC (Doles and Hemann, 2010; Ding et al., 2018). We wondered whether there was a circ-MEMO1-miR-485-3p-NEK4 axis in regulating propofol's role in LUAD.

Materials and methods

Cells

Human LUAD cell lines A549 (CRM-CCL-185; ATCC, Manassas, VA, USA) and H522 (CRL-5810; ATCC) were cultured in F-12K medium (Gibco, Grand Island, NY, USA) and RPMI-1640 medium (Gibco), respectively. Normal human bronchial epithelial cell line BEAS-2B (CL-0496; Procell, Wuhan, China) was cultured in the special BEGM medium (CM-0496; Procell). All cells were incubated in 90% heat-inactivated fetal bovine serum (Gibco) and a saturated humidity with 5% CO_2 at 37°C. Propofol (Sigma-Aldrich) was diluted in dimethylsulfoxide (DMSO; Sigma-Aldrich) for the store, and propofol (2, 4, and 8 μg/mL) was added in complete media of A549 and H522 cells for 24, 48, and 48 h. The 0.1% DMSO was added in A549 and H522 cells, serving as control of propofol treatment.

Cell viability assay

3-(4,5-dimethyl-2-thiazolyl)-2,5-diphenyl-2-H-tetrazolium bromide (MTT) method was utilized to measure cell viability of propofol-treated cells. 1×10^4 cells were seeded in a 96-well plate and cultured in complete medium added with 0, 2, 4, and 8 μg/mL propofol. At different time points (24 h, 48 h, and 72 h), the medium was changed with fresh medium containing 20 μL MTT reagent (5 mg/mL; Yeasen, Shanghai, China) for 4 h to generate intracellular water-insoluble formazan crystals which were then dissolved in DMSO (Sigma-Aldrich). The colorimetric analysis was measured at 490 nm on a microplate reader (Bio-Tek, Instruments, Neufahrn, Germany). Each reaction was run in triplicate to obtain the average value.

Cell cycle analysis

Flow cytometry (FCM) method was employed to analyze cell cycle phases. Cells were fixed with 70% cold ethanol and stained with 100 μg/mL propidium iodide (PI; (Sigma-Aldrich) supplemented with 50 μg/mL of RNase A (Sigma-Aldrich) in the dark. Then, stained DNAs were analyzed on a flow cytometer, and the proportion of cells in G0/G1, S, and G2/M phases was determined. Each reaction was run in triplicate to obtain the average value.

Cell proliferation assay

Cell-Light 5-ethynyl-2-deoxyuridine (EdU) Apollo567 *in Vitro* Kit (Ribobio, Guangzhou, China) was purchased to measure cell proliferation by detecting DNA replication activity. Cells in 96-well plate at 70% confluence were labeled with 100μL EdU (50 μM), immobilized with 4% paraformaldehyde, neutralized with 50 μL glycocoll (2 mg/mL), and stained with 100 μL of Apollo staining reaction (1×). After re-dyed with DAPI Staining Solution (Beyotime, Shanghai, China), fluorescence detections were visualized under fluorescence microscope (Nikon Microsystems, Shanghai, China), and the rate of EdU positive cells to DAPI-positive cells was calculated according to three random fields. Each reaction was run in triplicate to obtain the average value.

Migration and invasion assays

1×10^5 cells were harvested for migration and invasion assays using transwell Permeable Supports (8.0 μm; Corning, Cambridge, UK). For the invasion assay, the transwell support was pre-treated with 50 μL Matrigel Matrix (BD Biosciences, Franklin Lakes, NJ, USA). In the transwell systems, cell suspension in serum-free medium was loaded in the upper place, and serum-containing complete medium was added in the bottom place. Cells in the transwell system were further cultured for 48 h, and some cells were mechanically removed from the upper surface of the supports to the bottom surface. These transferred cells were visualized under the microscope after being stained with 0.2%

crystal violet solution (Beyotime). The number of the migrated/invaded cells was counted in eight fields of the transwell system.

Real-time quantitative PCR (qPCR) and western blotting

Human tissues and cells were lysed in TRIzol (Invitrogen, Carlsbad, CA, USA) for total RNAs isolation and in RIPA (Thermo Fisher Scientific, San Jose, CA, USA) for total proteins extraction. RNAs were reverse transcribed to cDNA using HiScript II 1st Strand cDNA Synthesis Kit (Vazyme, Nanjing, China), and RNA expression was detected in qPCR assay using specific primers and ChamQ SYBR Color qPCR Master Mix (Vazyme). The sequence of primers for circ-MEMO1, miR-485-3p, NEK4, β-actin, and U6 was shown in Table 1. The relative RNA expression was calculated using the $2^{-\Delta\Delta Ct}$ method with normalization to β-actin or U6. Proteins expression was measured by western blotting method. In brief, proteins were separated by sodium dodecyl sulfate-polyacrylamide gel electrophoresis and then transferred onto polyvinylidene fluoride membranes. The membranes carrying proteins were successive incubated with 5% skim milk, primary antibodies, and secondary antibodies. With ECL detection kit (Thermo Fisher Scientific), chemiluminescence was captured on chemiluminescence capture system (Bio-Rad Laboratories, Hercules, CA, USA) and quantified by Image Lab™ software (Bio-Rad Laboratories). The relative protein levels were normalized to β-actin. Primary antibodies were CyclinD1 (sc-8396; 1:1,000, Santa Cruz, Dallas, TX, USA), E-cadherin (sc-8426; 1:1,000, Santa Cruz), Vimentin (sc-6260; 1:1,000, Santa Cruz), β-actin (sc-47778; 1:500, Santa Cruz), and NEK4 (sc-81332; 1:500, Santa Cruz); secondary antibody was m-IgGκ BP-HRP (sc-516102; 1:10,000, Santa Cruz).

Table 1. The sequences of primers, shRNAs, siRNAs, and miRNAs.

Name	Sequence (5'-3')
circ-MEMO1 primer (177 bp)	GCAGACAGATGAAGATGAACACA AGGGGCACATGATGAGAAGG
miR-485-3p primer (73 bp)	TACACGGCTCTCCTCTCTGT TGTCGTGGAGTCGGCAATTG
NEK4 primer (112 bp)	GAAGCCCAGCTCTTGTCTCA CACCTCCTTCACAGAAGCCC
β-actin primer (104 bp)	CTTCGCGGGCGACGAT CCACATAGGAATCCTTCTGACC
U6 primer (72 bp)	GCGCGTCGTGAAGCGTTC GTGCAGGGTCCGAGGT
sh-circ-MEMO1	AUGGAAAGCCAUGCAGGAUAU AUAUCCUGCAUGGCUUUCCAU
sh-NC	UUCUCCGAACGUGUCACGU ACGUGACACGUUCGGAGAA
si-NEK4	CUGAAUUGUUCUCAAACAAAC UUGUUUGAGAACAAUUCAGGG
si-NC	UUCUCCGAACGUGUCACGU
miR-485-3p	GUCAUACACGGCUCUCCUCUCU
miR-NC	ACGUGACACGUUCGGAGAATT
anti-miR-485-3p	AGAGAGGAGAGCCGUGUAUGAC
anti-miR-NC	UUCUCCGAACGUGUCACGUTT

Patients

In the Affiliated Hospital of Hebei University, 52 primary LUAD patients were recruited and no patient had received local or systemic treatment before operation. After the written consents collection, tumor tissues and peri-cancer tissues were collected and soaked in liquid nitrogen. These patients were submitted to surgery operation between 2014.4 and 2020.3. This study was approved by the Institutional Research Ethics Committee of Affiliated Hospital of Hebei University and experiments were executed according to the Declaration of Helsinki Principles. Clinicopathological variables of 52 LUAD patients and their association with circ-MEMO1 expression had been shown in Table 2.

Cell transfection

A549 and H522 cells were subjected to cell transfection. For overexpression, circ-MEMO1 overexpression vector based on the pCD-ciR vector (Geneseed Biotech, Guangdong, China) and commercial miR-485-3p mimic (miR-485-3p) were obtained. For knockdown, short interfering RNA (shRNA) against circ-MEMO1 (sh-circMEMO1), small interfering RNA (siRNA) targeting NEK4 (si-NEK4), and commercial

Table 2. Association of circ-MEMO1 expression with clinicopathological variables in LUAD.

Characteristics	n	circ-MEMO1 expression		p value
		High(n=26)	Low(n=26)	
Gender				0.158
Female	21	8	13	
Male	31	18	13	
Age (years)				0.244
<60	18	7	11	
≥60	34	19	15	
Tumor Size				0.012
≥3	25	17	8	
<3	27	9	18	
Tumor stage				0.025
I+II	30	11	19	
III+IV	22	15	7	
Lymph node metastasis				0.001
Yes	20	16	4	
No	32	10	22	
Differentiation grade				0.071
Well/moderately	36	15	21	
Poorly	16	11	5	

miR-485-3p inhibitor (anti-miR-485-3p) were obtained, as well as negative controls miR-NC, sh-NC, si-NC and anti-miR-NC. The sequence of these nucleotides is shown in Table 1. Cell transfection was performed at 70% cell density and using Lipofectamine RNAiMAX reagent (Invitrogen) as instructed. After transfection for 6 h, A549 and H522 cells were treated with 8 μg/mL propofol for 48 h prior to functional assays. DMSO (0.1%) alone served as control.

Dual-luciferase reporter assay

The full length of 3'untranslated region (3'UTR) of NEK4 covering the wild-type (WT) miR-485-3p target sequences were generated from NEK4 RNA (NM_003157.6) and inserted into luciferase report vector pGL4 (Promega, Madison, WI, USA). Similarly, the circ-MEMO1-WT sequence was cloned into pGL4 (Promega). The sites UGUAUGA in circ-MEMO1-MUT and NEK4 3'UTR-WT were mutated into ACAUACU using a PCR-based approach, and circ-MEMO1-MUT and NEK4 3'UTR-MUT report vectors were generated. A549 and H522 cells were co-transfected with the above pGL4 constructs and commercial miR-485-3p or miR-NC for 48 h. Luciferase activity of the reporter vectors was determined using the Dual-Luciferase system (Promega) as instructed. The luciferase activity normalized to the protein concentration was expressed as a ratio of *Firefly* luciferase to *Renilla* luciferase units.

Statistical analysis

All experiments were conducted in triplicate. The results were presented as the mean ± standard deviation, and statistical significances were determined by one-way analysis of variance or Student's t-test. Statistical analysis was performed using a software package (GraphPad Prism 6.0; GraphPad La Jolla, CA, USA). Kaplan-Meier method was used for survival analysis. Differences were considered statistically significant at $P<0.05$.

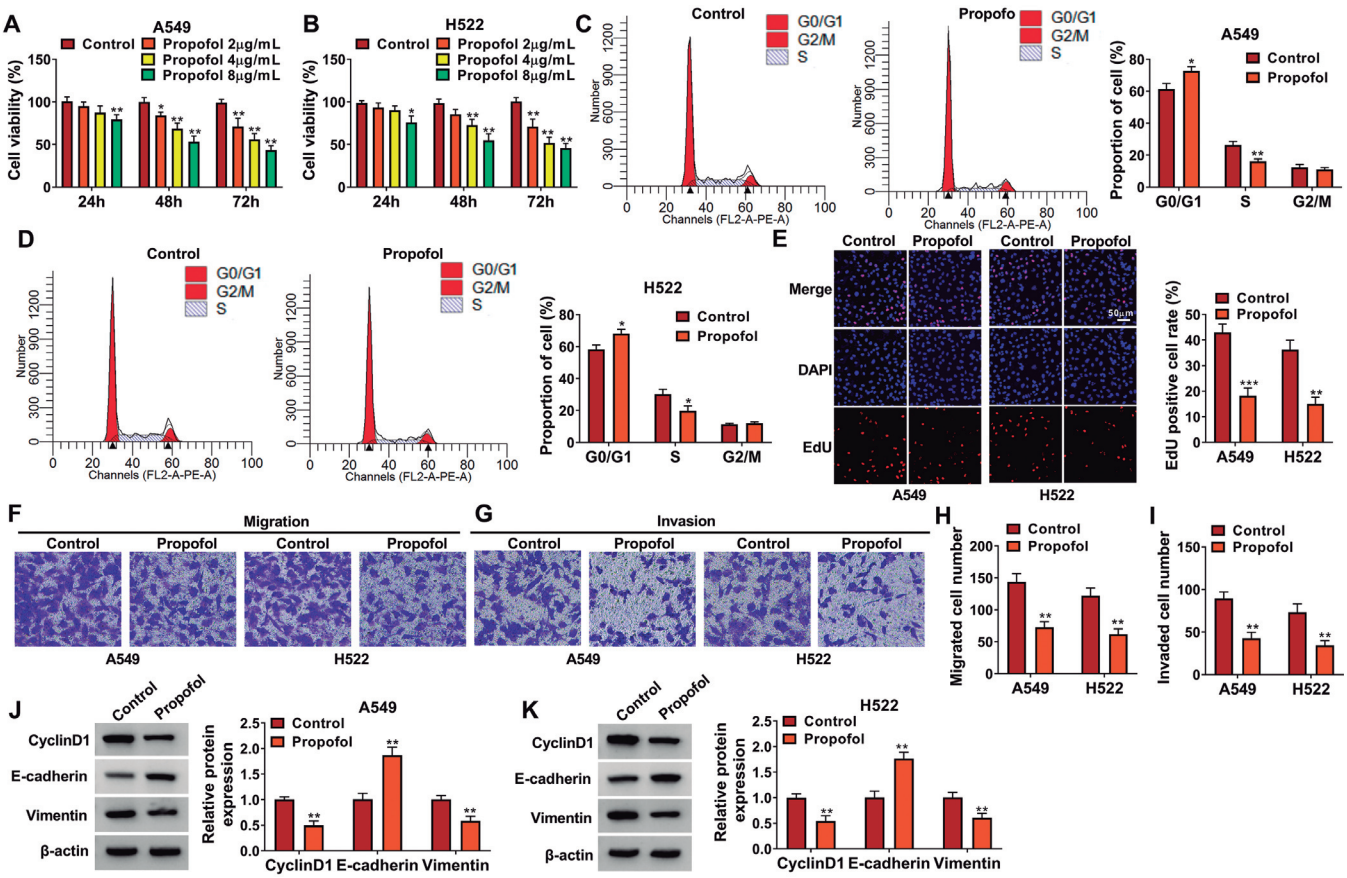

Fig. 1. Propofol curbed LUAD cell growth, migration, and invasion *in vitro*. **A, B.** MTT assay measured cell viability (%) of A549 and H522 cells treated with different concentrations of propofol for 24 h, 48 h, and 72 h. **C-K.** A549 and H522 cells were treated with 8 μg/mL propofol for 48 h, compared with control cells (without propofol treatment). **C, D.** FCM method detected the proportion of cells in different cell cycle phases G0/G1, S and G2/M. **E.** EdU assay estimated the rate of EdU positive cells in DAPI-positive cells. **F, G.** Transwell assays showed cell migration and invasion. **H, I.** Transwell migrated cell numbers and invaded cell numbers were counted. **J, K.** Western blotting examined the protein expression of CyclinD1, E-cadherin, and Vimentin, with normalization to β-actin. *P<0.05, **P<0.01 and ***P<0.001. F, G, x 100.

Results

Propofol anesthesia curbed LUAD cell growth and metastasis in vitro

Propofol treatment impaired cell viability of LUAD A549 and H522 cells (Fig. 1A,B), and this inhibition was in a dose- and time-dependent manner. As a result, 8 μg/mL propofol anesthesia at 48 h caused about 50% cell viability inhibition in both cells (Fig. 1A,B). Thus, A549 and H522 cells anesthetized with 8 μg/mL propofol anesthesia for 48 h were harvested for further detections. FCM method showed that cells distributed in the S phase were reduced, and G0/G1 phase cells were accumulated with propofol anesthesia (Fig. 1C,D), which was paralleled with depressed CyclinD1 expression (Fig. 1J,K). EdU assay revealed that propofol anesthesia could lower EdU positive cell rate in A549 and H522 cells (Fig. 1E). Transwell migrated cell number and invaded cell number were both declined in response to propofol treatment (Fig. 1F-I), accompanied with increased E-cadherin expression and inhibited Vimentin expression (Fig. 1J,K). These results together demonstrated a suppressive role of propofol in LUAD cell growth and metastasis *in vitro*.

Circ-MEMO1 and miR-485-3p were abnormally expressed in LUAD patients

Analysis of qPCR was employed to detect differently expressed RNAs in LUAD patients. Expression of circ-EMEO1 was higher, whereas miR-485-3p was lower in LUAD tumor tissues than paired normal tissues (Fig. 2A,C). Of note, there were inverse linear correlations between miR-485-3p and circ-MEMO1 expression in 52 LUAD tumors (Fig. 2D). Besides, high circ-MEMO1 was associated with low 5-year overall survival in this cohort of patients (Fig. 2B), as well as tumor size, TNM stage, lymph node metastasis, and differentiation grade (Table 2). These outcomes showed the dysregulations of circ-MEMO1, miR-485-3p, and NEK4 in LUAD patients, suggesting that they might display potential roles in LUAD cells in an interactive way.

Overexpression of circ-MEMO1 hampered tumor-suppressive role of propofol in LUAD cells

Compared with normal BEAS-2B cells, A549 and H522 cells highly expressed circ-MEMO1 (Fig. 3A), and this expression was suppressed with propofol anesthesia (Fig. 3B). Forcedly, circ-MEMO1 expression was further overexpressed in A549 and H522 cells using overexpression vector transfection (Fig. 3C). Overexpression of circ-MEMO1 was executed together with propofol anesthesia in A549 and H522 cells. As a result, propofol-induced inhibitions of cell viability and cell cycle entrance to S phase were prohibited with circ-MEMO1 overexpression vector transfection (Fig. 3D,E). EdU positive cell rate and CyclinD1 expression in

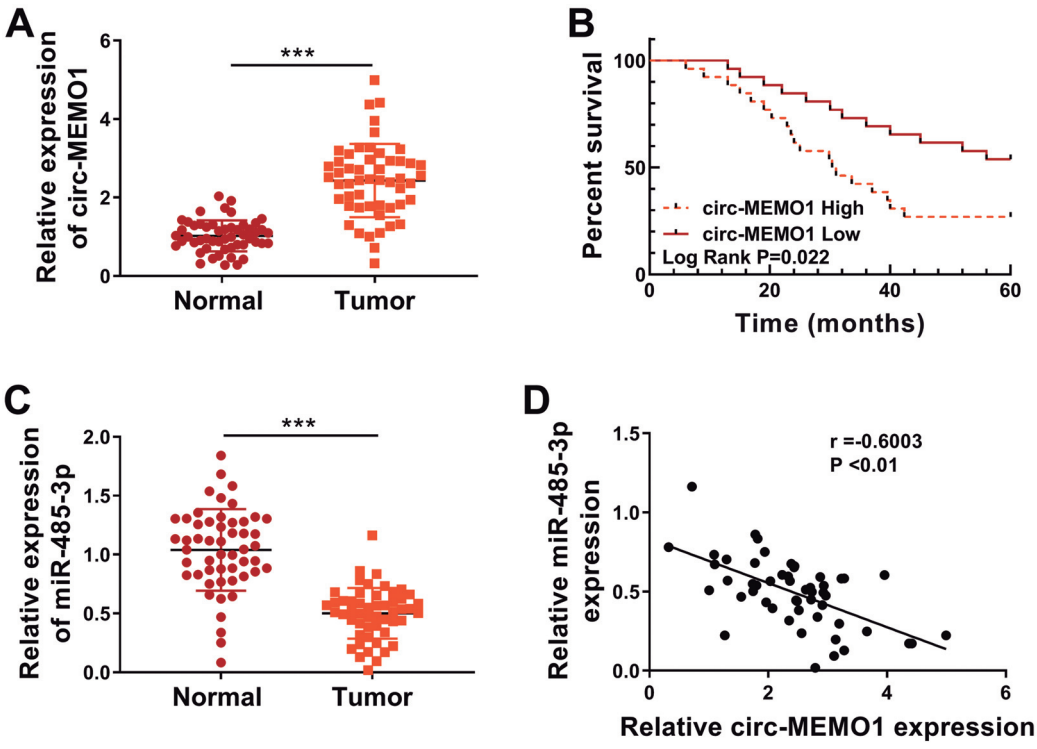

Fig. 2. The dysregulations of circ-MEMO1, miR-485-3p, and NEK4 in LUAD patients. **A, C.** qPCR detected expression of circ-MEMO1 and miR-485-3p in LUAD tumor tissues (Tumor; n=52) and para-carcinoma normal tissues (Normal; n=52). **B.** Kaplan-Meier method analyzed the percent of overall survival of 52 LUAD patients divided into two groups: circ-MEMO1 High (n=26) and circ-MEMO1 Low (n=26). **D.** Pearson's correlation analysis confirmed the relationship between circ-MEMO1 and miR-485-3p expression in LUAD tumors. ***P<0.001.

propofol-anesthetized A549 and H522 cells were rescued with circ-MEMO1 overexpression (Fig. 3F-G and 3J-3K). The anti-metastasis role of propofol in A549 and H522 cells was also salvaged by introducing circ-MEMO1 overexpression vector, as evidenced by the improvements of migrated/invaded cell numbers and Vimentin expression (Fig. 3H-K), as well as the reduction of E-cadherin expression (Fig. 3J,K). These data showed that overexpressing circ-MEMO1 could hamper the anti-LUAD role of propofol *in vitro*.

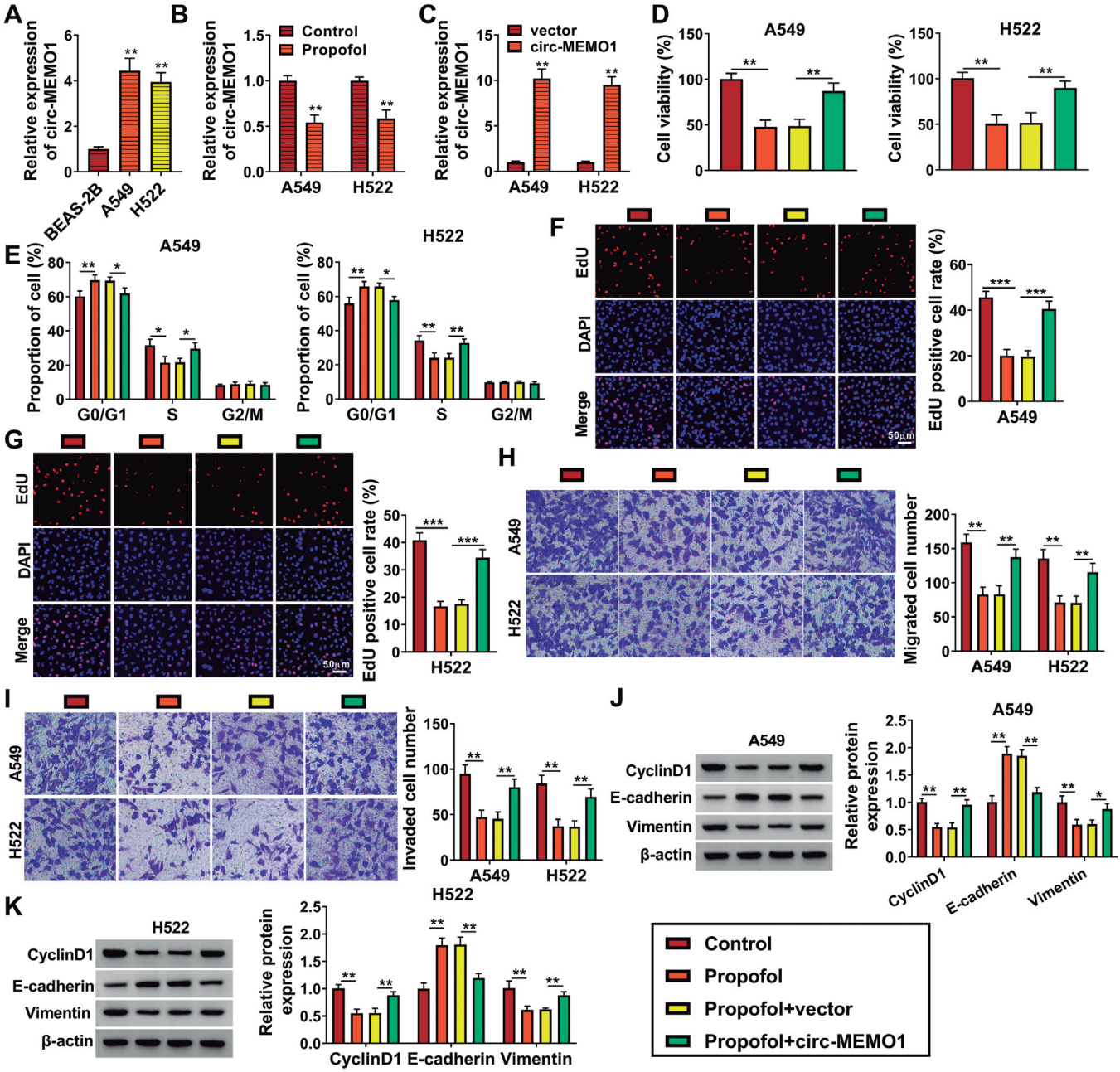

Fig. 3. Overexpression of circ-MEMO1 hampered tumor-suppressive role of propofol in LUAD cells. **A-C.** qPCR detected circ-MEMO1 expression in BEAS-2B **(A)**, A549 and H522 cells, A549 and H522 cells treated with 8 μg/mL propofol or not **(B)**, and A549 and H522 cells transfected with circ-MEMO1 overexpression vector (circ-MEMO1) or empty vector **(C)**. **D-K.** A549 and H522 cells were treated with 8 μg/mL propofol solely or together with vectors transfection. **D.** MTT assay measured cell viability (%). **E.** FCM method detected the proportion of cells in G0/G1, S, and G2/M phases. **F, G.** EdU assay estimated EdU positive cell rate. **H, I.** Transwell assays showed migrated cell numbers and invaded cell numbers. **J, K.** Western blotting examined the protein expression of CyclinD1, E-cadherin and Vimentin, normalized to β-actin. *P<0.05, **P<0.01 and ***P<0.001. H, I, x 100.

There was an interaction between circ-MEMO1 and miR-485-3p

CircBank, Circinteractome, and starbase algorithms were together used to predict miRNAs response elements in circ-MEMO1, and two computational target miRNAs were obtained (Fig. 4A). Ectopic expression of circ-MEMO1 caused downregulation of miR-485-3p, and contrarily its knockdown via shRNA provoked miR-485-3p upregulation in A549 and H522 cells (Fig. 4B-D); meanwhile, miR-337-3p expression was unresponsive to circ-MEMO1 different expression. Thus, the predicted binding sites of miR-485-3p in circ-MEMO1 were mutated to examine the potential interaction between circ-MEMO1 and miR-485-3p (Fig. 4E). Mimic transfection could overexpress miR-485-3p in A549 and H522 cells (Fig. 4F), and miR-485-3p overexpression could attenuate luciferase activity of circ-MEMO1-WT report vector instead of the MUT vector (Fig. 4G,H). These outcomes indicated that circ-MEMO1 could sponge miR-485-3p via target binding. Expression of miR-485-3p was downregulated in A549

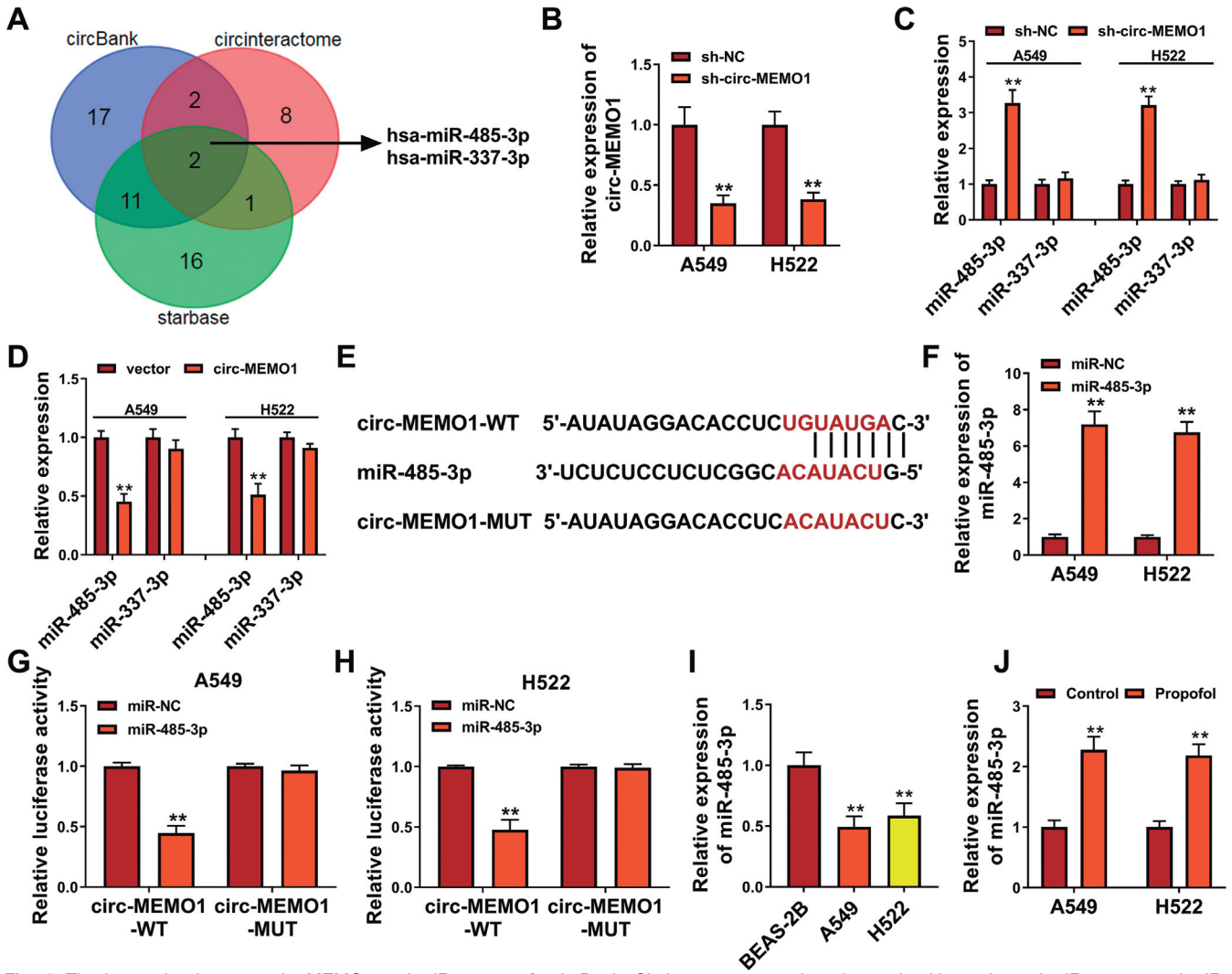

Fig. 4. The interaction between circ-MEMO1 and miR-485-3p. **A.** circBank, Circinteractome, and starbase algorithms showed miR-485-3p and miR-377-3p as computational targets for circ-MEMO1. **B.** qPCR detected transfection efficiency of sh-circ-MEMO1 in A549 and H522 cells by analyzing circ-MEMO1 expression, compared with sh-NC transfection. **C, D.** qPCR detected miR-485-3p and miR-377-3p expression in A549 and H522 cells transfected with sh-NC, sh-circ-MEMO1, vector or circ-MEMO1 vector. **E.** The computational binding sites of miR-485-3p in the sequence of circ-MEMO1-WT were shown, as well as their mutations in the sequence of circ-MEMO1-MUT. **F.** qPCR detected transfection efficiency of commercial miR-485-3p in A549 and H522 cells by analyzing miR-485-3p expression, compared with miR-NC transfection. **G, H.** Dual-luciferase reporter assay determined luciferase activity of circ-MEMO1-WT vector and circ-MEMO1-MUT vector in A549 and H522 cells transfected with miR-485-3p or miR-NC. **I, J.** qPCR detected miR-485-3p expression in BEAS-2B, A549, and H522 cells **(I)**, and A549 and H522 cells treated with 8 μg/mL propofol or not **(J)**. **P<0.01.

and H522 cells (Fig. 4I), but this expression level could be upregulated by propofol anesthesia (Fig. 4J).

Hyperexpression of miR-485-3p partially countermanded the impacts of circ-MEMO1 on propofol role in LUAD cells

To further determine whether there was an interactive effect between circ-MEMO1 and miR-485-3p in regulating LUAD cell progression, rescue experiments were performed, and LUAD A549 and H522 cells were divided into four groups: propofol+vector, propofol+circ-MEMO1, propofol+circ-MEMO1+miR-NC, and propofol+circ-MEMO1+miR-485-3p. Overexpression of circ-MEMO1 via transfection was conducive to cell growth of LUAD cells under propofol anesthesia, while this growth-promoting role could be diminished with co-transfection with miR-485-3p, as described by the loss of cell viability, S phase cells and EdU positive cell rate (Fig. 5A-C), as well as the increase of G0/G1 phase cells (Fig. 5B). According to transwell assays, cell migration and invasion of propofol-anesthetized A549 and H522 cells were promoted due to circ-MEMO1 overexpression, and this pro-metastasis role was counteracted in the co-presence of miR-485-3p (Fig. 5D,E). Molecularly, introducing miR-485-3p, expression of CyclinD1 and Vimentin was descended, and E-cadherin was augmented in circ-

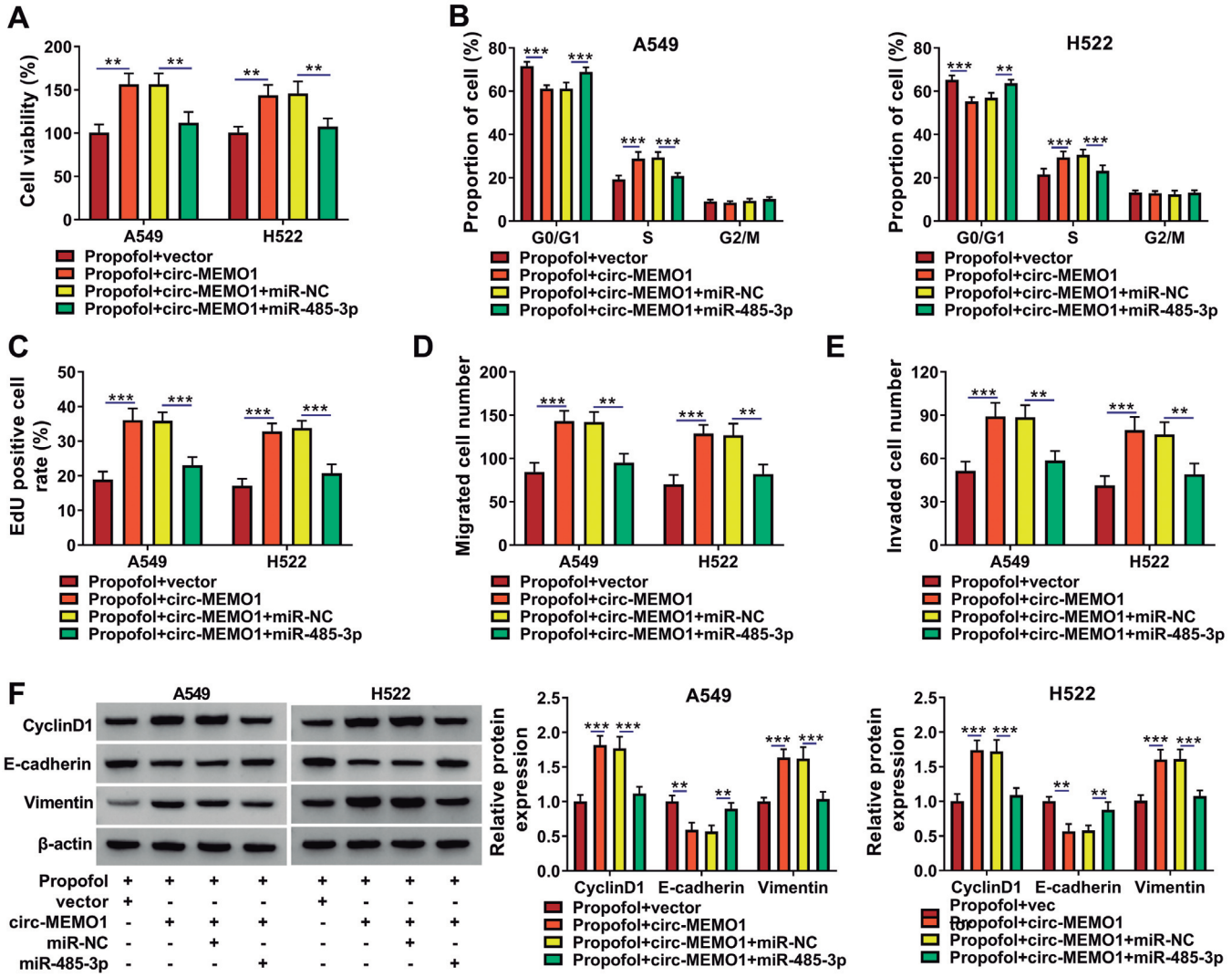

Fig. 5. Hyperexpression of miR-485-3p partially countermanded the impacts of circ-MEMO1 on propofol's role in LUAD cells. **A-F.** A549 and H522 cells were co-treated with 8 μg/mL propofol and transfection of vectors alone or combined with miRNAs. **A.** MTT assay measured cell viability (%). **B.** FCM method detected the proportion of cells in G0/G1, S, and G2/M phases. **C.** EdU assay estimated EdU positive cell rate. **D, E.** Transwell assays showed migrated cell numbers and invaded cell numbers at 100×. **F.** Western blotting examined the protein expression of CyclinD1, E-cadherin and Vimentin, normalized to β-actin. **P<0.01 and ***P<0.001.

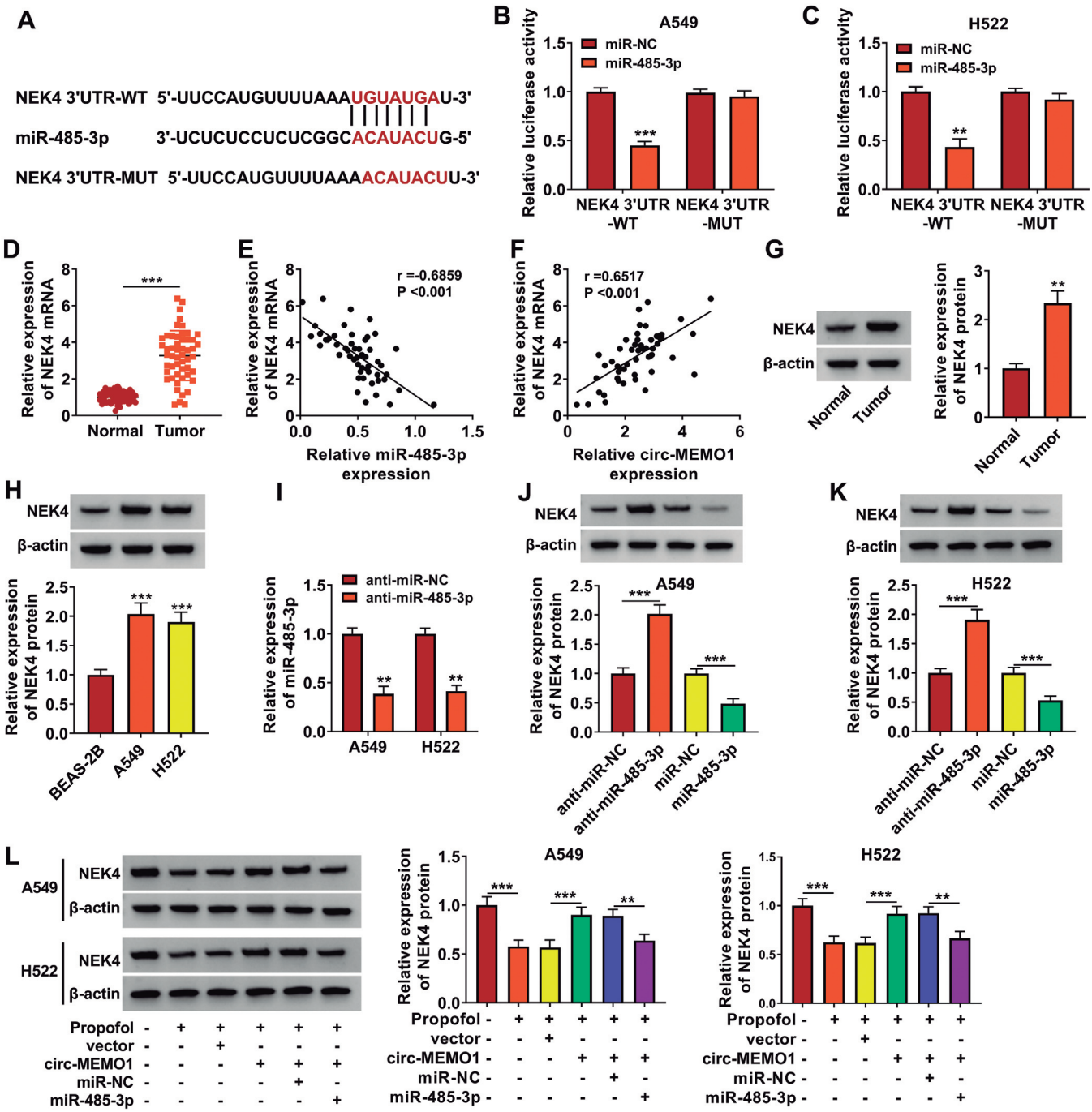

Fig. 6. The interplay between circ-MEMO1-miR-485-3p and NEK4. **A.** The miR-485-3p-binding sites and their mutations were shown in the NEK4 3'UTR-WT sequence and NEK4 3'UTR-MUT sequence, respectively. **B, C.** Dual-luciferase reporter assay determined luciferase activity of NEK4 3'UTR-WT vector and NEK4 3'UTR-MUT vector in A549 and H522 cells transfected with miR-485-3p or miR-NC. **D.** qPCR detected expression of NEK4 mRNA in LUAD tumor tissues (Tumor; n=52) and para-carcinoma normal tissues (Normal; n=52). **E, F.** Pearson's correlation analysis confirmed the relationship between NEK4 mRNA and miR-485-3p or circ-MEMO1 expression in LUAD tumors. **G, H.** Western blotting detected NEK4 protein expression in Tumor tissues, Normal tissues, LUAD A549 and H522 cells, and normal BEAS-2B cells. **I.** qPCR examined miR-485-5p expression to evaluate transfection efficiency of anti-miR-485-3p in A549 and H522 cells compared to anti-miR-NC. **J-L.** Western blotting detected NEK4 protein expression in A549 and H522 cells **(J, K)** transfected with anti-miR-NC, anti-miR-485-3p, miR-NC, or miR-485-3p, and co-treated with 8 μg/mL propofol and transfections of vectors alone or along with miRNAs **(L)**. **P<0.01 and ***P<0.001.

MEMO1-overexpressed A549 and H522 cells under propofol anesthesia (Fig. 5F). These results validated that miR-485-3p hyperexpression could partially countermand the adverse impacts of circ-MEMO1 overexpression on propofol protection in LUAD cells against malignant growth and metastasis.

There was an interaction between circ-MEMO1-miR-485-3p and NEK4

Starbase software also showed potential miR-485-3p binding sites in NEK4 3'UTR (Fig. 6A). As expected, dual-luciferase reporter assay identified the responsiveness of miR-485-3p overexpression on NEK4 3'UTR-WT report vector rather than the MUT report vector (Fig. 6B,C). NEK4 mRNA expression was upregulated in 52 LUAD patients' tissues than paired normal tissues (Fig. 6D), and there was an inverse linear correlation between miR-485-3p and NEK1 mRNA expression and a positive linear correlation between circ-MEMO1 and NEK1 mRNA expression in these LUAD cases (Fig. 6E,F). Additionally, NEK4 protein was also highly induced in LUAD tumors and cells (Fig. 6G,H). In addition, NEK4 protein expression could be upregulated and downregulated with miR-485-3p deficiency and hyperexpression via transfection, respectively (Fig. 6I-K). Furthermore, the NEK4 protein level in propofol-treated LUAD cells could be upregulated by ectopic circ-MEMO1, and this upregulation could be diminished by miR-485-3p (Fig. 6L). These data depicted a direct interaction between miR-485-3p and NEK4, and an interaction among circ-MEMO1, miR-485-3p, and NEK4 in LUAD cells.

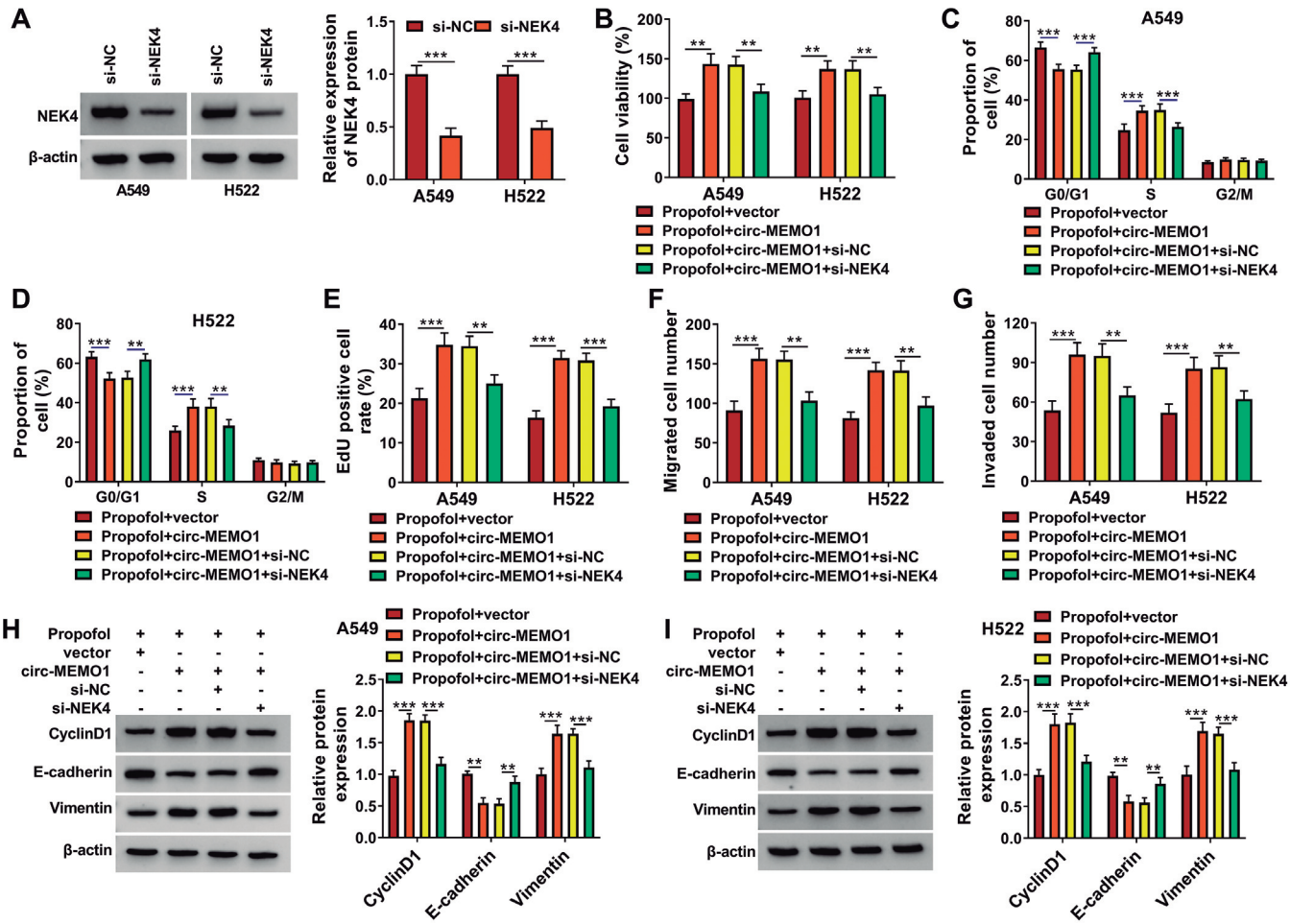

Fig. 7. Knockdown of NEK4 weakened the impacts of circ-MEMO1 on propofol's role in LUAD cells. **A.** Western blotting examined NEK4 protein expression to evaluate transfection efficiency of si-NEK4 in A549 and H522 cells compared to si-NC. **B-F.** A549 and H522 cells were co-treated with 8 μg/mL propofol and transfections of vectors alone or combined with siRNAs. **B.** MTT assay measured cell viability (%). **C, D.** FCM method detected the proportion of cells in G0/G1, S, and G2/M phases. **E.** EdU assay estimated EdU positive cell rate. **F, G.** Transwell assays showed migrated cell numbers and invaded cell numbers at 100×. **H, I.** Western blotting examined the protein expression of CyclinD1, E-cadherin and Vimentin, normalized to β-actin. **P<0.01 and ***P<0.001.

Knockdown of NEK4 weakened the impacts of circ-MEMO1 on propofol role in LUAD cells

The interactive effect between circ-MEMO1 and NEK4 in regulating LUAD cell progression was further figured out in rescue experiments in A549 and H522 cells that were divided into four groups: propofol+vector, propofol+circ-MEMO1, propofol+circ-MEMO1+si-NC, and propofol+circ-MEMO1+si-NEK4. Western blotting data demonstrated a high transfection efficiency of si-NEK4 in both A549 and H522 cells (Fig. 7A). The si-NEK4-mediated silencing of NEK4 partially but significantly diminished the overall effects of circ-MEMO1 overexpression on cell viability, cell cycle progression, EdU incorporation, migration, invasion, and expression of marker proteins in propofol-anesthetized A549 and H522 cells (Fig. 7B-I). These findings demonstrated the weakening of NEK4 knockdown on circ-MEMO1 overexpression role in LUAD cells under propofol treatment *in vitro*.

Discussion

Mounting evidence showed that cancer growth, metastasis, recurrence, and drug resistance could be overall inhibited by propofol (Jiang et al., 2018b; Xu et al., 2020), and propofol exerted anti-tumor potential partly due to suppressing several circRNAs, such as circ-PVT1, circTADA2A, and circRNA001372 (Sui et al., 2020; Wang et al., 2020; Zhao et al., 2020). Here, we identified that circ-MEMO1 was a novel propofol-related circRNA in LUAD and circ-MEMO1 downregulation might contribute to propofol-induced inhibiting effects on growth, migration, and invasion of LUAD cells *in vitro* via MEMO1-miR-485-3p-NEK4 competing endogenous RNA (ceRNA) axis (Fig. 8).

In this study, circ-MEMO1 was highly expressed in LUAD patients' tumors and cells compared to adjacent non-tumor tissues and cells. In terms of circ-MEMO1 expression status in NSCLC, Jiang et al. (Jiang et al., a2018) screened circRNA expression profile in NSCLC tissues and found that circ-MOM1 was one of the most differently upregulated circRNAs in NSCLC tissues. Next, upregulation of circ-MEMO1 was successively observed in different groups of human NSCLC tumors and diverse NSCLC cell lines (Ding et al., 2020; Lin et al., 2020; Ye et al., 2020), as well as exosomes from NSCLC patients' serum (Ding et al., 2020). Clinically, higher circ-MEMO1 in tissues and/or serum exosomes might predict a heavier tumor burden and poor survival in NSCLC patients (Ding et al., 2020; Lin et al., 2020; Ye et al., 2020). Moreover, we observed that circ-MEMO1 expression in LUAD cells was responsive to propofol anesthesia and downregulated. Concerning functional roles, overexpression of circ-MEMO1 was contributing to cell viability, cell cycle progression, cell proliferation, migration, and invasion of LUAD cells under propofol treatment *in vitro*. These results altogether demonstrated that circ-MEMO1 overexpression could damage propofol-induced anti-growth and anti-metastasis effects in LUAD cells; coincidentally, propofol disrupted lung cancer carcinogenesis by depressing not only circ-MEMO1 (in this study) but also circTADA2A (Zhao et al., 2020). By the way, the oncogenic role of circ-MEMO1 in NSCLC had previously been revealed both *in vitro* and *in vivo* using loss-of-function experiments.

Earlier studies illustrated that propofol exerted anti-tumor potential partly due to regulating the expression and transfer of miRNAs (Zhang et al., 2014; Zheng et al., 2020). Herein, we noticed that miR-485-3p was suggested as a promising target for circ-MEMO1 according to three bioinformatics algorithms, and miR-485-3p expression status was sensitive to circ-MEMO1

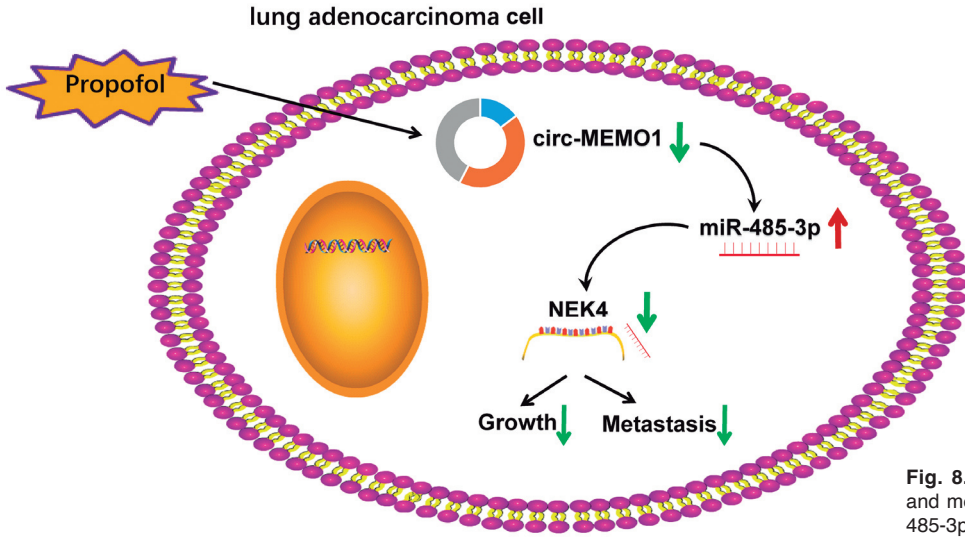

Fig. 8. Propofol suppressed LUAD cell growth and metastasis *in vitro* via the circ-MEMO1-miR-485-3p-NEK4 axis.

dysregulation in LUAD cells. Furthermore, the predicted binding sites of miR-485-3p in circ-MEMO1 were responsive to miR-485-3p overexpression in dual-luciferase reporter assay, suggesting a direct interaction between circ-MEMO1 and miR-485-3p. What's more, miR-485-3p expression was detected to be downregulated in these LUAD patients' tissues and cells. Furthermore, the downregulation of miR-485-3p in NSCLC tumors (than peri-tumor tissue) and NSCLC cells (than normal BEAS-2B cells) was consistent with the existing research (Gao and Ye, 2020). In this study, we find out that the basal low expression of miR-485-3p in LUAD cells could be highly elevated in response to propofol anesthesia, and its overexpression via mimic contributed to deficient growth, migration, and invasion of circ-MEMO1-overexpressed LUAD cells under propofol anesthesia. Functionally, the tumor-suppressive role of miR-485-3p had been uncovered in different malignant tumors, such as osteosarcoma, breast cancer, and prostate cancer (Formosa et al., 2014; Lou et al., 2016; Wang et al., 2021a,b). In NSCLC, existing evidence showed that miR-485-3p deficiency diminished lncRNA SNHG6 silencing-mediated both promotion of apoptosis and suppression of proliferation, migration, and invasion in NSCLC H520 and H596 cells (Gao and Ye, 2020). Nevertheless, whether miR-485-3p functioned as a tumor suppressor in NSCLC cells had not been directly and convincingly confirmed yet. Plus, miR-485-3p was still a less-documented miRNA in human cancers.

Next, NEK4 was identified as a target gene for miR-485-3p and its expression could be modulated by circ-MEMO1-miR-485-3p interaction in LUAD cells. In LUAD patients, NEK4 mRNA and protein were consistently upregulated in tumor tissues versus para-tumor tissues; moreover, NEK4 mRNA expression in LUAD patients' tumors was significantly correlated to circ-MEMO1 and miR-485-3p. Paralleled with miR-485-3p restoration via mimic, NEK4 exhaustion via siRNA could decrease growth, migration, and invasion of circ-MEMO1-overexpressed LUAD cells under propofol anesthesia. These data suggested that circ-MEMO1 knockdown hampered propofol's anti-LUAD role by promoting miR-485-3p-targeted NEK4. Previous documents well depicted the close linkage of oncogene NEK4 to NSCLC apoptosis and metastasis both *in vitro* and *in vivo* (Doles and Hemann, 2010; Park et al., 2016; Ding et al., 2018; Elsocht et al., 2021). Of note, NEK4 is a potent target in the treatment of NSCLC, and developing a selective inhibitor of NEK4 could be beneficial to prolong the life of the patients (Doles and Hemann, 2010; Elsocht et al., 2021).

In terms of the dose and duration of propofol, 2-10 μg/mL propofol were performed for 1-3 days in human gastric and lung cancers for *in vitro* cell study (Sui et al., 2020; Zhao et al., 2020). Additionally, there was a study that demonstrated an alteration of lung cancer A549 cell proliferation by 1 h-propofol treatment at a low concentration of 2 μg/mL (Sun and Gao, 2018); while lung cancer A549 and H1299 cell viabilities were also observed not to be affected by 2 μg/mL propofol for a long time of 48 h (Sun and Gao, 2018; Zhao et al., 2020). Our data showed that 2 μg/mL propofol treatment could reduce lung cancer A549 and H522 cell viability for at least 48 h, and the high doses of propofol at 8 μg/mL. could affect these cells at 24 h. Collectively, the researches focusing on the dose and duration of propofol's anti-tumor role *in vitro* cells are non-uniform, and thus more studies are warranted to be performed. By the way, a high dose of propofol (8 μg/mL, 48 h) has been widely used to measure the malignant behaviors of lung cancer cells (Sun and Gao, 2018; Wu et al., 2020; Zhao et al., 2020), including this present study. However, whether 8 μg/mL. Propofol could affect A549 and H522 cells at 12 h, 8 h, 4 h, etc. remain to be further measured in this study. Besides, Sun and Gao, 2018 indicated that 8 μg/mL Propofol treatment for 48 h could not affect normal lung epithelial BEAS-2B cells, but a higher concentration of propofol at 10 μg/mL was detrimental to BEAS-2B cells (Sun and Gao, 2018). In terms of *in vivo* experiments of propofol's anti-tumor effect, nude mice were given an intraperitoneal injection of propofol at a dose of 20-35 mg/kg once a day or every 3 days for 15-20 days (Zhang et al., 2014; Sui et al., 2020; Zheng et al., 2020); additionally, intratumoral injection method was also attempted to treat xenograft tumor of A549 cells by propofol (Zhao et al., 2020). While the association between the circ-MEMO1-miR-485-3p-NEK4 axis and propofol's anti-LUAD role was warranted to be validated *in vivo* experiment in the near further.

In conclusion, we demonstrated that propofol anesthesia suppressed LUAD cell growth and metastasis by downregulating circ-MEMO1, and overexpression of circ-MEMO1 could abate propofol-induced anti-LUAD role by guiding miR-485-3p and NEK4. This work suggested that the circ-MEMO1-miR-485-3p-NEK4 ceRNA pathway was one underlying mechanism of propofol's tumor-inhibiting role in LUAD.

Acknowledgements. None.

Disclosure of interest. The authors declare that they have no conflicts of interest.

Funding. None.

Ethics approval and consent participate. Written informed consent was obtained from patients with approval by the Institutional Review Board in Affiliated Hospital of Hebei University.

Consent for publication. Not applicable.

Author Contribution. Lei Chen had full access to all of the data in the study and takes responsibility for the integrity of the data and the accuracy of the data analysis. Study concept and design: Lei Chen, Guangyi Wu, Yongle Li; acquisition of data: Guangyi Wu, Yongle Li and Qiaoying Cai; critical revision of the manuscript for important intellectual content: Lei Chen, Guangyi Wu; administrative, technical or material support: Lei Chen, Guangyi Wu, Yongle Li; study supervision: Lei Chen.

Data Availability Statement. Please contact the correspondence author for the data request.

References

Beermann J., Piccoli M.T., Viereck J. and Thum T. (2016). Non-coding rnas in development and disease: Background, mechanisms, and therapeutic approaches. Physiol. Rev. 96, 1297-1325.

Cassinello F., Prieto I., del Olmo M., Rivas S. and Strichartz G.R. (2015). Cancer surgery: How may anesthesia influence outcome?. J. Clin. Anesth. 27, 262-272.

Ding N.H., Zhang L., Xiao Z., Rong Z.X., Li Z., He J., Chen L., Ou D.M., Liao W.H. and Sun L.Q. (2018). NEK4 kinase regulates EMT to promote lung cancer metastasis. J. Cell. Mol. Med. 22, 5877-5887.

Ding C., Xi G., Wang G., Cui D., Zhang B., Wang H., Jiang G., Song J., Xu G. and Wang J. (2020). Exosomal circ-MEMO1 promotes the progression and aerobic glycolysis of non-small cell lung cancer through targeting miR-101-3p/KRAS axis. Front. Genet. 11, 962.

Doles J. and Hemann M.T. (2010). NEK4 status differentially alters sensitivity to distinct microtubule poisons. Cancer Res. 70, 1033-1041.

Elsocht M., Giron P., Maes L., Versees W., Gutierrez G.J., De Greve J. and Ballet S. (2021). Structure-activity relationship (SAR) study of spautin-1 to entail the discovery of novel NEK4 inhibitors. Int. J. Mol. Sci. 22.

Farooqi A.A., Adylova A., Sabitaliyevich U.Y., Attar R., Sohail M.I. and Yilmaz S. (2020). Recent updates on true potential of an anesthetic agent as a regulator of cell signaling pathways and non-coding RNAs in different cancers: Focusing on the brighter side of propofol. Gene 737, 144452.

Formosa A., Markert E.K., Lena A.M., Italiano D., Finazzi-Agro E., Levine A.J., Bernardini S., Garabadgiu A.V., Melino G. and Candi E. (2014). MicroRNAs, miR-154, miR-299-5p, miR-376a, miR-376c, miR-377, miR-381, miR-487b, miR-485-3p, miR-495 and miR-654-3p, mapped to the 14q32.31 locus, regulate proliferation, apoptosis, migration and invasion in metastatic prostate cancer cells. Oncogene 33, 5173-5182.

Gao N. and Ye B. (2020). SPI1-induced upregulation of lncRNA SNGH6 promotes non-small cell lung cancer via miR-485-3p/VPS45 axis. Biomed. Pharmacother. 129, 110239.

Giordano M., Boldrini L., Servadio A., Niccoli C., Melfi F., Lucchi M., Mussi A. and Fontanini G. (2018). Differential microRNA expression profiles between young and old lung adenocarcinoma patients. Am. J. Transl. Res. 10, 892-900.

Irwin M.G., Chung C.K.E., Ip K.Y. and Wiles M.D. (2020). Influence of propofol-based total intravenous anaesthesia on peri-operative outcome measures: A narrative review. Anaesthesia 75 (Suppl. 1), e90-e100.

Ishola A.A., La'ah A.S., Le H.D., Nguyen V.Q., Yang Y.P., Chou S.J., Tai H.Y., Chien C.S. and Wang M.L. (2020). Non-coding RNA and lung cancer progression. J. Chin. Med. Assoc. 83, 8-14.

Jiang M.M., Mai Z.T., Wan S.Z., Chi Y.M., Zhang X., Sun B.H. and Di Q.G. (2018a). Microarray profiles reveal that circular RNA hsa_circ_0007385 functions as an oncogene in non-small cell lung cancer tumorigenesis. J. Cancer Res. Clin. Oncol. 144, 667-674.

Jiang S., Liu Y., Huang L., Zhang F. and Kang R. (2018b). Effects of propofol on cancer development and chemotherapy: Potential mechanisms. Eur. J. Pharmacol. 831, 46-51.

Kim R. (2017). Anesthetic technique and cancer recurrence in oncologic surgery: Unraveling the puzzle. Cancer Metastasis Rev. 36, 159-177.

Liang Z.Z., Guo C., Zou M.M., Meng P. and Zhang T.T. (2020). CircRNA-miRNA-mRNA regulatory network in human lung cancer: An update. Cancer Cell Int. 20, 173.

Lin Y., Su W. and Lan G. (2020). Value of circular RNA 0007385 in disease monitoring and prognosis estimation in non-small-cell lung cancer patients. J. Clin. Lab. Anal. 34, e23338.

Longhini F., Bruni A., Garofalo E., De Sarro R., Memeo R., Navalesi P., Navarra G., Ranieri G., Curro G. and Ammendola M. (2020). Anesthetic strategies in oncological surgery: Not only a simple sleep, but also impact on immunosuppression and cancer recurrence. Cancer Manag. Res. 12, 931-940.

Lou C., Xiao M., Cheng S., Lu X., Jia S., Ren Y. and Li Z. (2016). MiR-485-3p and miR-485-5p suppress breast cancer cell metastasis by inhibiting PGC-1alpha expression. Cell Death Dis. 7, e2159.

Ng W.L., Mohd Mohidin T.B. and Shukla K. (2018). Functional role of circular RNAs in cancer development and progression. RNA Biol. 15, 995-1005.

Park S.J., Jo D.S., Jo S.Y., Shin D.W., Shim S., Jo Y.K., Shin J.H., Ha Y.J., Jeong S.Y., Hwang J.J., Kim Y.S., Suh Y.A., Chang J.W., Kim J.C. and Cho D.H. (2016). Inhibition of never in mitosis a (nRNA)-related kinase-4 reduces survivin expression and sensitizes cancer cells to trail-induced cell death. Oncotarget 7, 65957-65967.

Sahinovic M.M., Struys M. and Absalom A.R. (2018). Clinical pharmacokinetics and pharmacodynamics of propofol. Clin. Pharmacokinet. 57, 1539-1558.

Santos R.M., Moreno C. and Zhang W.C. (2020). Non-coding RNAs in lung tumor initiation and progression. Int. J. Mol. Sci. 21.

Sui H., Zhu C., Li Z. and Yang J. (2020). Propofol suppresses gastric cancer tumorigenesis by modulating the circular RNA-PVT1/miR1955p/E26 oncogene homolog 1 axis. Oncol. Rep. 44, 1736-1746.

Sun H. and Gao D. (2018). Propofol suppresses growth, migration and invasion of A549 cells by down-regulation of miR-372. BMC Cancer 18, 1252.

Wang J., Cheng C.S., Lu Y., Ding X., Zhu M., Miao C. and Chen J. (2018). Novel findings of anti-cancer property of propofol. Anticancer Agents Med. Chem. 18, 156-165.

Wang M., Suo L., Yang S. and Zhang W. (2021a). CircRNA 001372 reduces inflammation in propofol-induced neuroinflammation and neural apoptosis through PIK3CA/Akt/NF-kappaB by miRNA-148b-3p. J. Invest. Surg. 34, 1167-1177.

Wang Q., Liu M.J., Bu J., Deng J.L., Jiang B.Y., Jiang L.D. and He X.J. (2021b). Mir-485-3p regulated by MALAT1 inhibits osteosarcoma glycolysis and metastasis by directly suppressing c-MET and AKT3/mTOR signalling. Life Sci. 268, 118925.

Wu X., Li X. and Xu G. (2020). Propofol suppresses the progression of nonsmall cell lung cancer via downregulation of the miR215p/MAPK10 axis. Oncol. Rep. 44, 487-498.

Xu Y., Pan S., Jiang W., Xue F. and Zhu X. (2020). Effects of propofol on the development of cancer in humans. Cell Prolif. 53, e12867.

Ye Y., Zhao L., Li Q., Xi C., Li Y. and Li Z. (2020). Circ_0007385 served as competing endogenous RNA for miR-519d-3p to suppress malignant behaviors and cisplatin resistance of non-small cell lung cancer cells. Thorac. Cancer 11, 2196-2208.

Zhang J., Shan W.F., Jin T.T., Wu G.Q., Xiong X.X., Jin H.Y. and Zhu S.M. (2014). Propofol exerts anti-hepatocellular carcinoma by microvesicle-mediated transfer of miR-142-3p from macrophage to cancer cells. J. Transl. Med. 12, 279.

Zhao H., Wei H., He J., Wang D., Li W., Wang Y., Ai Y. and Yang J. (2020). Propofol disrupts cell carcinogenesis and aerobic glycolysis

by regulating circTADA2a/miR-455-3p/FOXM1 axis in lung cancer. Cell Cycle 19, 2538-2552.

Zheng X., Dong L., Zhao S., Li Q., Liu D., Zhu X., Ge X., Li R. and Wang G. (2020). Propofol affects non-small-cell lung cancer cell biology by regulating the miR-21/PTEN/AKT pathway *in vitro* and *in vivo*. Anesth. Analg. 131, 1270-1280.

Accepted May 6, 2022